Magnetization measurements on ITER Nb_3Sn CICC and strands subjected to irreversible strain degradation

2012 Supercond. Sci. Technol. 25 075004

(http://iopscience.iop.org/0953-2048/25/7/075004)

Supercond. Sci. Technol. **25** (2012) 075004 (9pp) doi:10.1088/0953-2048/25/7/075004

Magnetization measurements on ITER Nb_3Sn CICC and strands subjected to irreversible strain degradation

C Zhou[1], D Bink[1], B Liu[2], Y Miyoshi[1], W A J Wessel[1], H J G Krooshoop[1] and A Nijhuis[1]

[1] Faculty of Science and Technology, University of Twente, Energy, Materials and Systems (EMS), Enschede, The Netherlands
[2] Institute of Plasma Physics, Chinese Academy of Sciences, Superconducting Magnet and Energy Saving Centre, Hefei, People's Republic of China

E-mail: c.zhou@utwente.nl

Received 24 February 2012, in final form 20 April 2012
Published 22 May 2012
Online at stacks.iop.org/SUST/25/075004

Abstract
We investigated the impact of irreversible strain changes and filament cracking on the AC losses of several Nb_3Sn strands and a full-size ITER cable-in-conduit-conductor (CICC). The aim is to evaluate whether the presence of filament cracks in full-size ITER Nb_3Sn CICC (after cyclic loading) can be detected without extracting strands from the cable for microscopic observation. The strand AC loss was measured in a magnetometer in virgin condition and after an applied periodic and cyclic bending strain. The filament fracture pattern was determined afterwards by SEM analysis.

We found a significant decrease of the hysteresis loss in ITER bronze and internal-tin type strands with increasing filament fracture density. However, in the experimental comparison between a highly degraded section of a full-size ITER TF CICC sample subjected to high electromagnetic load and a section taken from the low magnetic field zone, no clear difference is observed in hysteresis loss but only in coupling loss.

The first measurement on a full-size ITER CICC sample indicates that the amount of cracks is at least restricted to an average crack density of 0.05 cracks/filament/mm but a higher accuracy of the CICC AC loss measurement is required for better precision. Further work is required to evaluate whether the observed degradation of the current sharing temperature and *n*-value is essentially attributed to strand deformation and associated periodic strain variations or filament cracks.

(Some figures may appear in colour only in the online journal)

1. Introduction

Superconducting materials in cabled high-current conductors are often subjected to high mechanical stresses arising from winding tension and bending strain during fabrication, differential thermal contraction between different materials and the Lorentz force when energizing a magnet [1]. In the ITER central solenoid (CS) and toroidal field (TF) magnet system, the cabled superconductors, composed of about thousand superconducting wires, experience high magnetic field (>12 T) and current (up to 68 kA). This leads to substantial transverse Lorentz forces [2], large strains and possibly filament breakage that reduce the transport properties [3].

The occurrence and distribution of filament cracks in full-size ITER Nb_3Sn samples after cyclic testing can be studied by strand polishing and scanning electron microscopy (SEM) [4, 5]. This method provides immediate quantitative

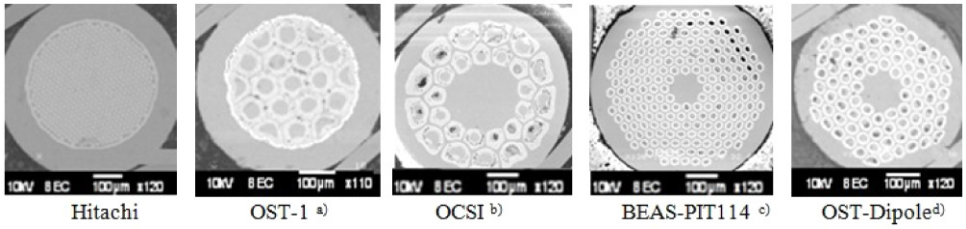

Figure 1. Cross-sectional photos of the investigated strands. (a) OST is produced by Oxford Superconducting Technology, USA. (b) OCSI is produced by Luvata, Italy. (c) BEAS is produced by Bruker Energy and Supercon Technologies (BEST), Germany. (d) The OST-Dipole Nb_3Sn strand, used for the EDIPO dipole coil presently under construction.

data on the count of cracks and their distribution inside the strands and corresponding location in the cable. Alternatively, a magnetization measurement could offer some advantages for investigating the overall presence of filament cracks in a full-size ITER CICC, and mainly for this reason we investigated the impact of filament cracking on the strand AC losses.

It was anticipated that, in particular, strands with filament bundles containing sintered links (or contacts) between filaments could be sensitive to a decrease of the magnetization with crack growth. The measured magnetization could then be reduced due to interruption of superconducting current loops, being eliminated by the cracks. In the case of a sufficiently strong dependency between hysteresis loss and crack initiation, this effect may then be applicable for evaluation of the crack concentration in large ITER conductors during or after (cyclic) testing of the transport properties. In order to compare strand geometries from different processing methods, we tested five strands made with the bronze (BR), internal-tin (IT), powder-in-tube (PIT), and restacked-rod-process (RRP) route (the RRP process is also an internal-tin type but will be distinguished in this paper because it leads to different properties). The AC loss versus frequency was measured in a magnetometer in virgin condition and after two levels of applied periodic bending strain. The choice of the levels of peak bending strain was based on the range used for the TARSIS bending tests at the University of Twente and the bending strain expected in ITER full-size conductors [6, 7]. The filament fracture pattern was obtained by microscopic observation (SEM) after polishing the AC loss samples, giving a direct correlation between the filament crack concentration and the AC losses.

Here we report for the first time that a significant reduction of the hysteresis loss is observed in ITER type bronze and internal-tin strands with increasing applied periodic peak bending strain (section 3) and filament crack growth (section 5). We compared the strand AC loss results with that from a highly degraded section of a full-size ITER TF sample subjected to high current and magnetic field and a section taken from the low magnetic field zone, indicated as TFPRO2-OST1 cut from the SULTAN (SUpraLeiter Test ANlage) sample after cyclic testing (section 6).

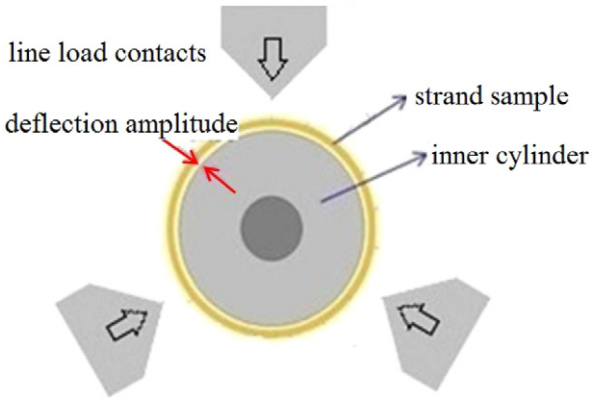

Figure 2. Schematic view of the three-point bending setup.

2. Strand characteristics and experimental setups

2.1. Strand samples

The tested Nb_3Sn strands were selected to have a wide variation in terms of processing techniques and manufacturers, e.g. bronze (Hitachi), internal-tin (OST-1 and OCSI), powder-in-tube (BEAS-PIT114) and restacked-rod-process (OST-Dipole) route. SEM micrographs of the cross-section of the investigated strands are shown in figure 1.

Each AC loss sample is prepared as a one-layer coil made up by 14 turns with an inner diameter of 40 mm, an outer diameter of 42 mm, a height of 14 mm and a sample wire length of 1800 mm. After the heat treatment the sample coils are supported by a thin layer of glass-fiber tape wound around the coil and impregnated with StycastTM epoxy.

2.2. Periodic bending setup

In order to apply periodic bending strain to a strand sample in a cyclic manner, a three-point press setup is used, as schematically shown in figure 2. The strand sample is placed around a cylinder with a diameter slightly smaller than the inner diameter of the strand sample. A bending strain is applied to the strand sample by moving the three line load contacts to the center until the surfaces of the inner cylinder and strand sample come into contact. The bending contacts are equidistantly distributed along the circumference of the coiled sample. After reaching the maximum deflection, the

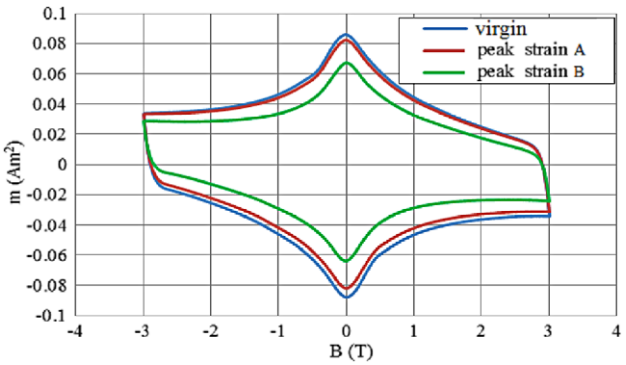

Figure 3. Magnetization as a function of applied field of OST-1 strand at $T = 4.2$ K, $B_a = 3$ T, $f = 10$ mHz.

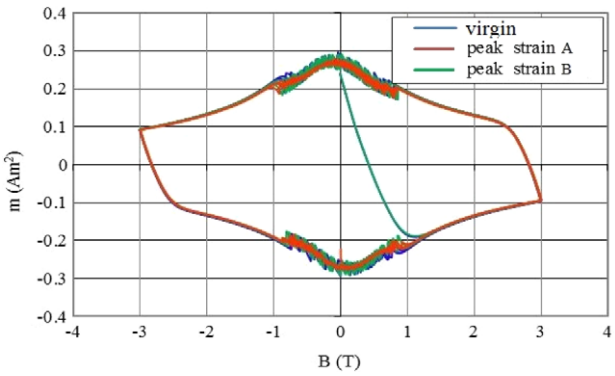

Figure 4. Magnetization as a function of applied field of OST-Dipole strand at $T = 4.2$ K, $B_a = 3$ T, $f = 10$ mHz.

force on the three line contacts is released and the strand sample is rotated around its central axis with an angle of 10° and the bending procedure is repeated. As a result, the strand sample is systematically loaded at 36 bending locations, which effectively involves a form of 12 times periodic bending.

Two inner cylinders are used with diameters of 38.5 and 36.9 mm, which limit the peak bending strain of the 41 mm diameter strand samples. The procedure of applying periodic bending strain with successive rotation of the sample is a cyclic process with locally varying applied peak bending strain and deflection amplitude. Therefore, we do not define a strain level associated with the applied deflection but refer to the applied load by A and B, corresponding to the two inner cylinders with diameters of 38.5 mm and 36.9 mm respectively.

2.3. AC losses and magnetization

The AC losses of all investigated strand specimens are measured in the virgin condition and after applied periodic peak bending deflection with cylinder A and B with the Twente magnetization measurement setup [8]. The setup uses a balanced pick-up coil-set [9] with a superconducting integrator [10] and offers a very high accuracy at low field ramping rates [6]. The strand AC loss measurements are carried out at liquid helium temperature (atmospheric pressure bath). The time varying magnetic field using a sinusoidal field sweep amplitude (B_a) of ±3 T around zero baseline is applied perpendicular to the specimen axis. In order to distinguish between hysteresis and coupling loss, the frequency (f) is varied from 2 to 25 mHz [11].

When no transport current is considered and only an external time varying magnetic field is applied to the sample, we assume that the hysteresis loss per cycle at low excitation ($f \sim 0$ Hz) is independent of the field frequency and the coupling loss can then be separated from the hysteresis loss by applying different frequencies [11, 12].

For a field cycle of amplitude $= 2B_a$, the coupling loss Q_c in terms of energy loss per unit volume and per applied field cycle can be written as:

$$Q_c = \frac{\pi B_a^2 \omega n\tau}{\mu_0}, \qquad (1)$$

where $n\tau$ is the effective coupling current loss time constant, which can be written as:

$$n\tau = \frac{\alpha \mu_0}{2\pi^2 B_a^2}, \qquad (2)$$

and α is the slope of the initial linear section of the total AC losses versus frequency (of identical amplitude) [11].

For the hysteresis loss component attributed to interfilament contacts (Q_{hc}) we may expect a relation as proposed in [13], where the dependence of Q_{hc} on the reciprocal characteristic length is described as $L_c^{-1} = L_p^{-1} + L_s^{-1}$. Here, L_p is the twist pitch and L_s is the sample length. In terms of Q_{hc}, samples with large L_p and small L_s, are equivalent to samples with small L_p and large L_s. This means that for L_p=15 mm, we do not expect a large decrease of the Q_{hc} with $L_s > 100$ mm. For a severe crack concentration, every 5 mm as imposed in our experiment, L_s would approach to 5 mm and the greatest part of this Q_{hc} loss component (75%) should be disrupted.

3. AC loss results

Typical results of the influence of imposed strain and filament cracking on the strand AC loss is illustrated by the magnetization curves in figures 3 and 4. The magnetization curve was measured as a function of the applied field at 4.2 K, with $B_a = 3$ T and $f = 10$ mHz, first in the virgin condition and repeated after applying periodic and cyclic bending strain with cylinders A and B respectively. A distinct decrease in the magnetization is observed for the OST-1 strand, in particular after the step in applied periodic bending strain with cylinder B (figure 3). However, for the OST-Dipole wire, with results shown in figure 4, no noticeable change in magnetization is perceived after bending. The results of the AC loss measurements with varying magnetic field frequency for the OST-1 and the OST-Dipole strand are plotted in figures 5 and 6. The slope of the linear fits through the data correspond to the coupling loss while the intercept at zero frequency reflects the hysteresis loss. The plots indicate that both the hysteresis and the coupling loss decrease significantly after applying periodic bending strain in the OST-1 type of strand. For the OST-Dipole wire, only the coupling loss reduces appreciably and the hysteresis loss reduces only marginally.

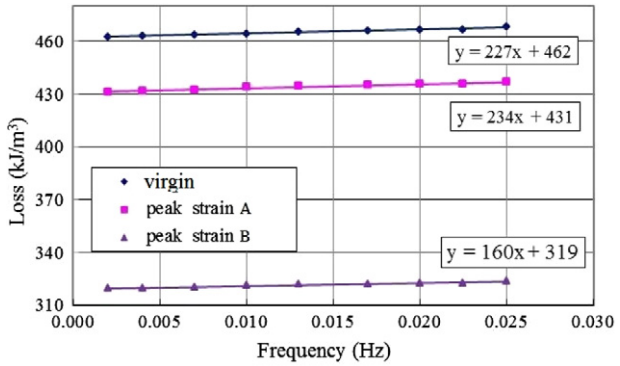

Figure 5. Total AC loss of OST-1 strand with $T = 4.2$ K, $B_a = 3$ T.

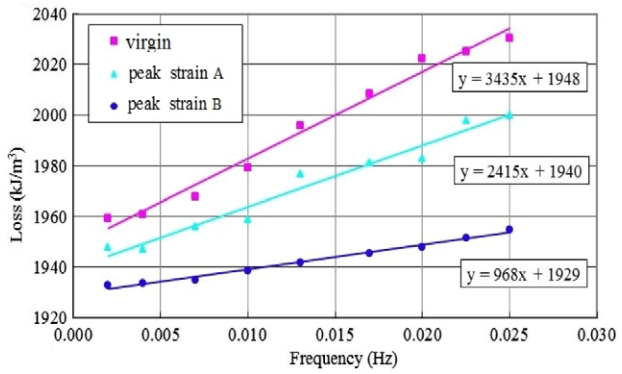

Figure 6. Total AC loss of OST-Dipole strand with $T = 4.2$ K, $B_a = 3$ T.

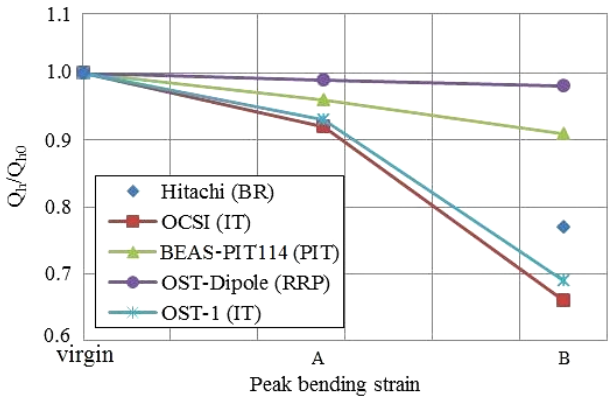

Figure 7. Hysteresis loss reduction versus applied periodic bending strain represented by cylinder A and B.

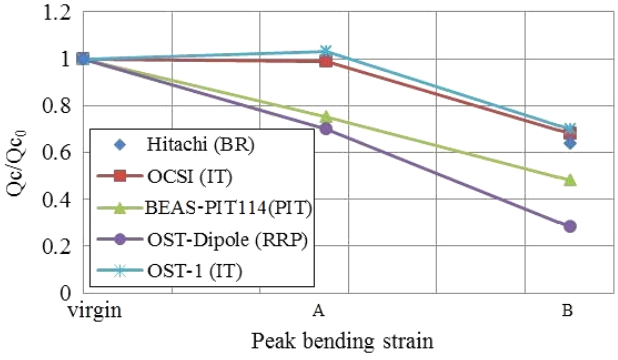

Figure 8. Coupling loss reduction versus applied periodic bending strain represented by cylinder A and B.

An overview of the reduction of the hysteresis and coupling loss for all investigated strands is plotted in figures 7 and 8. The figures illustrate a significant decrease of the hysteresis loss in the ITER bronze and internal-tin type wires (the Hitachi bronze strand is only tested in the virgin condition and after loading with the use of cylinder B). The hysteresis loss of the PIT and RRP wire types are evidently less sensitive to applied strain. For the coupling loss it is the other way around, as the PIT and RRP type of wires show a larger impact than the ITER type IT and BR wires. This opens the opportunity to explore AC loss measurement as a method to evaluate quantitatively the number of cracks in ITER type superconducting strands and full-size CICCs before and after application of an electromagnetic load. For clarity, the AC loss measurement in the SULTAN facility is not suitable for determination of the hysteresis loss because its frequency range does not allow accurate extrapolation to $f = 0$ Hz. Furthermore, unlike the hysteresis loss, the use of the coupling loss as a measure for the assessment of the presence of cracks in cabled conductors is not appropriate. That is because the reduction of interstrand coupling loss in Nb_3Sn CICCs subjected to electromagnetic loading will dominate the decrease of the intrastrand coupling loss due to crack initiation [14–16]. This implies that only measurement of the hysteresis loss conducted with sufficient accuracy in the low-frequency (mHz) range, as for example in the facility used for the test in Twente, can lead to a successful comparison.

4. Microscopic crack pattern

It is well-known that the filament micro-cracks affect the strand transport properties by reducing the critical current, since a crack can be considered as a small interruption having the resistive normal state [17–19]. In order to gain more insight into the mechanism of filament micro-crack initiation, concentration and propagation in the Nb_3Sn strands, but in particular its impact on the strand's AC losses, the crack pattern of the AC loss samples after application of bending strain with cylinder B were analyzed using SEM. The results are presented in this section.

4.1. Mechanical polishing

For microscopic study of a longitudinal cross-section, strand segments cut from virgin strand and the strained strand respectively were embedded in an epoxy punk and mechanically polished. The piece of virgin strand is used as a reference to confirm that cracks created by abrasion are not present after the final polishing stage. The epoxy was removed by etching with acid before cutting the sample in order to avoid cracks generated during cutting. Furthermore, monitoring the sample mount thickness in each polishing step facilitates ensuring that the damaged fracture generated in the previous step was entirely polished away [4].

Special care is taken during polishing to remove exactly half the thickness of the strand in order to study the center

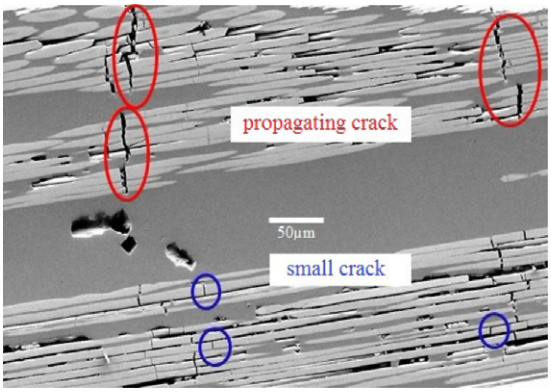

Figure 9. Micro-cracks of different orders observed in the polished longitudinal cross-section of the OST-1 (IT) strand after applied periodic peak bending strain with cylinder B.

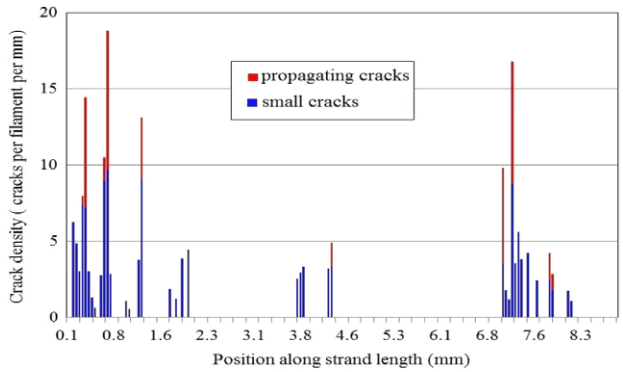

Figure 10. Distribution of the crack density along the strand length of the OST-1 (IT) strand after applied periodic peak bending strain with cylinder B.

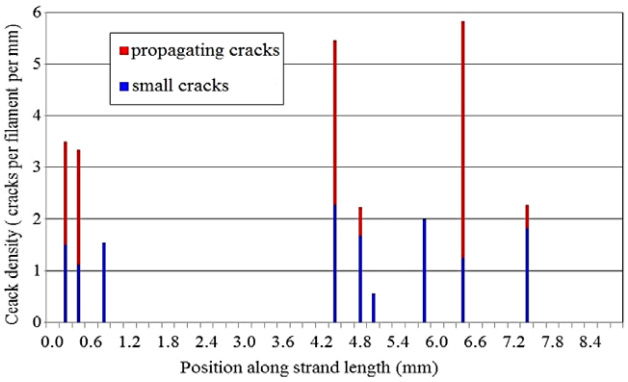

Figure 11. Distribution of the crack density along the strand length of the OST-Dipole (RRP) strand after applied periodic peak bending strain with cylinder B.

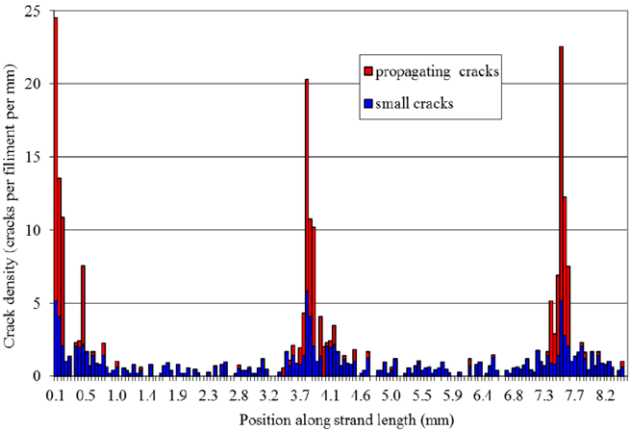

Figure 12. Distribution of the crack density along the strand length of the Hitachi (BR) strand after applied periodic peak bending strain with cylinder B.

of the strand. Final polishing is conducted with a 0.05 μm silica suspension in order to permit high-resolution imaging in the SEM. After that, the sample surface is lightly dip-etched in an HF–HNO_3 solution to remove the polishing deposit, to enhance micro-cracks without enlarging their size by controlling the etching time, and thus to better distinguish the microscopic fracture [4, 5]. SEM images are taken to identify the locations of the cracks, voids and filaments over the entire width of the filamentary region and with an axial sample length of 8–9 mm, which roughly corresponds to more than one periodic bending wavelength for all investigated strands.

4.2. Crack pattern

Here, micro-cracks we recognize are cracks that observably traverse at least one full filament width. The crack density is defined by counting the number of micro-cracks per filament per mm longitudinal length. Furthermore, cracks are categorized by the size of the region that they traverse, which should reflect and balance not only their destructive effect but also the impact on the AC loss. As illustrated in figure 9, we distinguish so-called small cracks, which are scattered, isolated and not propagated to neighboring filaments. At locations subjected to higher stresses, cracks in filaments are propagated to neighboring filaments or even through the whole filament bundle or filamentary region (propagating cracks).

Just as observed in previous studies [4, 20], the crack pattern varies appreciably for different strand types, as established in the histograms of the categorized crack density in figures 10–12. In comparison, in the IT (figure 10) and RRP (figure 11) strands and also the PIT strand with collective crack distribution, cracks are concentrated at the location with applied peak bending strain. The remainder of these strands is left highly crack free. This is in contrast to the well-distributed crack pattern shown in the bronze strand (figure 12), where there is no crack-free region between peak bending locations.

The average crack density for the OST-1 wire amounts to 1.0 cracks/mm/filament. For the OCSI (IT), BR, PIT and RRP strands the average crack density is 0.7, 1.8, 1.9 and 0.6 cracks/mm/filament respectively.

5. Crack pattern and AC loss

5.1. Interaction between cracks and hysteresis loss

Some multifilamentary Nb_3Sn strands exhibit hysteresis losses larger than what can be estimated by considering the actual filament dimension and superconductor critical

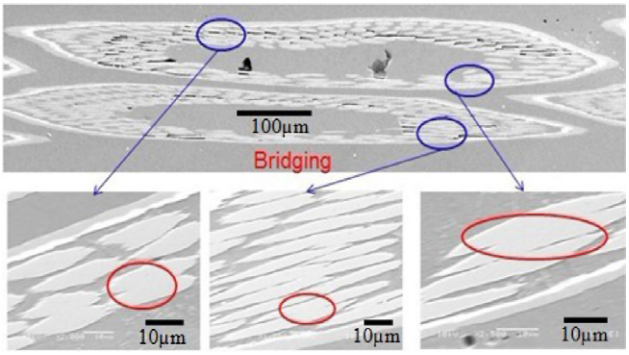

Figure 13. Bridging observed in polished longitudinal cross-section of OCSI (IT) strand.

current density, because interfilament coupling increases the so-called effective filament diameter. The effective filament diameter can be used as a measure of the hysteresis loss and can be significantly larger than the actual filament size due to bridging among filaments in IT strands (see figure 13) [21–23].

In wires made by the internal-tin diffusion process, it has been ascribed to bridging between filaments. The normal matrix in a multifilamentary wire shows weak superconductivity due to proximity coupling when the interfilamentary spacing is of the order of the normal coherence length. The coupling current generated by the proximity effect gives rise to an additional magnetization. Twisting also reduces the time-independent proximity effect between the filaments and its associated loss contribution.

It is very likely that in the tested IT strands, cracks reduce the effective filament diameter for hysteresis loss due to breaking of the superconducting loops that were established by the bridging among filaments. This is thought to lead to the relatively high reduction (over 30%) of the hysteresis loss in the two tested ITER type IT strands, reflecting correspondence to a significant fraction of the Q_{hc}.

Moreover, in the PIT type of strand the large filaments are not linked by bridging and so no large decrease of the hysteresis loss is expected. For the RRP type of strand, containing 84 bundles with 104 fine filaments per bundle, the filaments belonging to the same bundle are not only proximity coupled but also interlinked by sintering as one 'big filament'. In figure 7, we can see that the decrease of the hysteresis loss remains limited to less than 3% for the RRP type of strand after being subjected to the largest bending load. The small reduction may partly be caused by a decrease of the critical current due to the strand deformation, meanwhile creating a periodic bending strain distribution variation. However, with no evidence of bridging in the PIT type of strand, we still observe 9% reduction of the hysteresis loss. As illustrated in figure 14, in the RRP type of strand the cracks are highly concentrated around the locations with peak bending strain, but in the PIT strand the cracks are more widely distributed, with a width of more than 200 μm in the region around the peak bending strain. In that region, cracks separate the hollow filaments into short pieces (less than 50 μm) in the longitudinal direction, with many filament segments even smaller than their diameter. We believe this could be the main reason for the 9% reduction in hysteresis loss, as the path for the magnetization currents is drastically limited in these highly loaded areas, resulting in a smaller effective filament diameter.

The reduction in hysteresis loss of the BR strand is close to that from the IT strands. However, in the BR strand we did not find clear evidence of bridging from our microscopic observations, but the statistics of our analysis is rather limited. To a certain extent, the periodic bending partly separates the strand sample into pieces with a length corresponding to that of the periodic bending wavelength. A similar phenomenon was reported in [24], where the magnetization of a bronze route strand depends significantly on the sample length for samples shorter than one twist pitch, and it was suggested that interfilament contacts could play a role here, although we could not confirm this hypothesis by our SEM analysis. However, in [25] it was reported that for a similar BR strand, only a very small fraction of the filaments (1.8%) were merged after the HT, which would increase the 'effective filament diameter' probably only very marginally. This suggests that bridging for this type of BR strand has only very limited impact on the effective (hysteresis loss) filament diameter.

On the other hand, we definitely found a large number of longitudinal cracks inside the filaments in both virgin and strained BR strand, as shown in figure 15, and this was also reported previously in [25]. The longitudinal cracks seem to initiate from the unreacted Nb core in the filaments, probably leading to stress concentrations at the boundary layers and mostly propagating across the whole Nb_3Sn layer. The combination of longitudinal and transverse cracks generated by periodic bending splits one filament into several pieces. That also reduces not only the real filament dimensions but at the same time the effective filament diameter, leading to hysteresis loss reduction. After comparing the density and size of the longitudinal cracks in the virgin strand to that of longitudinal cracks in the strained strand, we found that both are larger after loading. This is indicated in figure 16, where small and large longitudinal cracks can be distinguished and accordingly defined as having a length shorter or longer than 20 μm respectively.

5.2. Interaction between cracks and coupling loss

Large crack events change the coupling current loops and reduce the coupling loss more than well-distributed crack events. The coupling loss reduction in PIT and RRP strands with thick filaments is larger than that in BR and IT strands (see figure 8). As illustrated in figure 17, large cracks break the coupling current loop into smaller loops with lower induced coupling current. On the other hand, small cracks do not change the main path of the coupling current loop but mainly increase the effective transverse resistance with R_{crack}.

In general, with highly concentrated large cracks around the location of the peak bending strain, the periodic bent strands can be considered as having an effective twist pitch

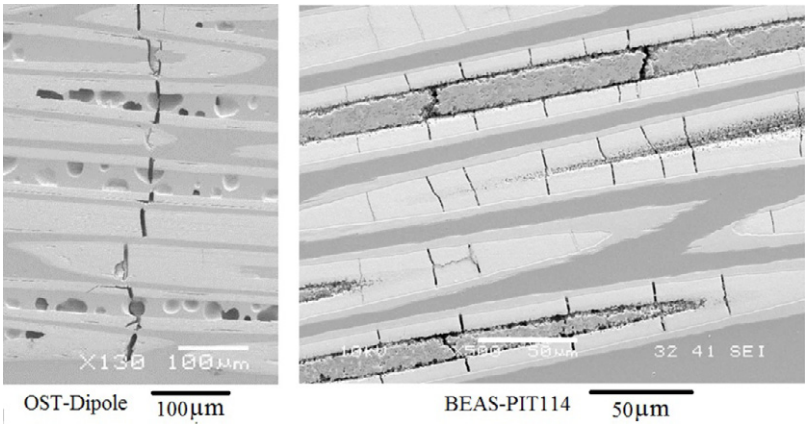

Figure 14. Crack pattern in OST-Dipole (RRP) and BEAS-PIT114 (PIT) strands.

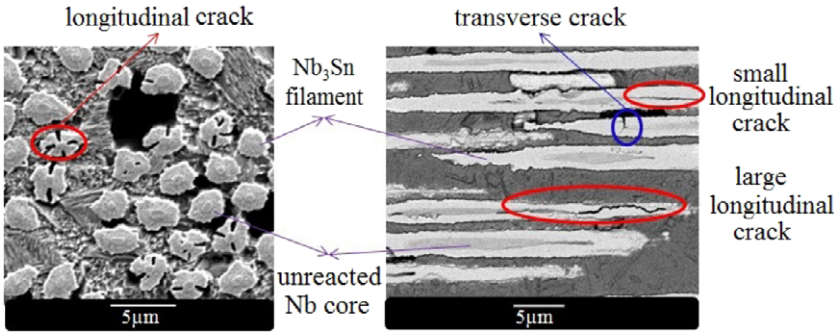

Figure 15. Longitudinal and transverse cracks, observed in polished transverse (left) and longitudinal (right) cross-sections of the BR strand.

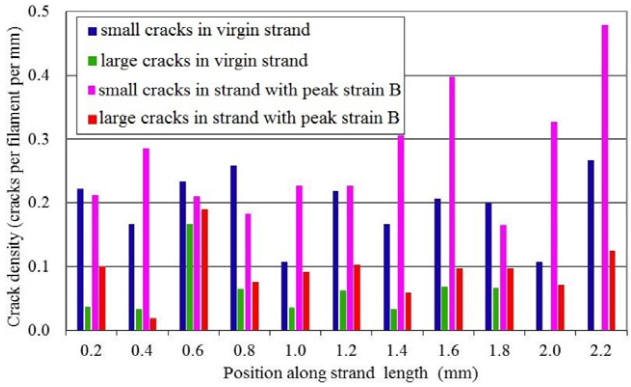

Figure 16. Distribution of longitudinal crack density along the strand length for the BR strand in the virgin state and periodically strained strand (with cylinder B).

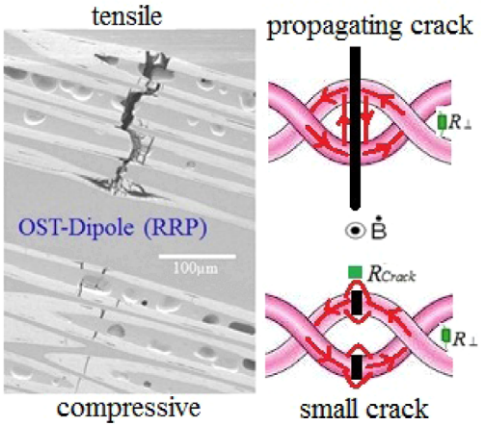

Figure 17. Scheme of the coupling current loops for large (top) and small cracks (bottom). The arrows represent the main current flow, $R_\perp$ is the coupling transverse resistance, and R_{crack} is the local resistance generated by a filament crack.

equal to the periodic bending wavelength, as the wavelength is shorter than the twist pitch in all tested strands [13, 26]. As a result, a shorter effective twist pitch leads to a lower coupling loss.

The IT strands with a more collective crack distribution show a similar coupling loss decrease to the BR strand. This may be explained by the large number of interfilament bridges (see figure 13) weakening the crack's destructive effect on the coupling loss.

6. AC loss of cycled ITER TF conductor

The findings of this work can be directly applied to investigate the influence of cyclic electromagnetic loading, possibly accompanied by filament fracture, on the hysteresis loss of a full-size ITER TF type of conductor. For this purpose, two sections of a full-size ITER TF sample, indicated as TFPRO2-OST1 are cut by spark erosion from the SULTAN

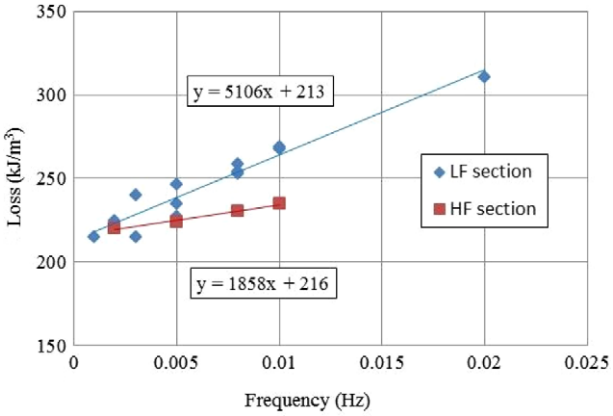

Figure 18. Magnetic AC loss measurement results of full-size ITER TF sample (OST-1) subjected to high field (HF) and low field (LF).

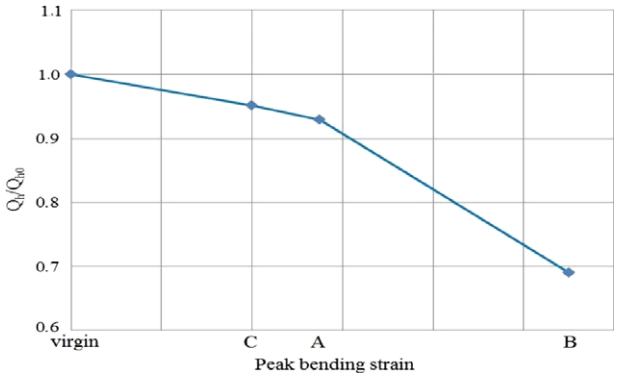

Figure 19. Hysteresis loss reduction versus applied periodic bending strain in the OST-1 wire represented by cylinder A and B and an additional cylinder C with a larger diameter of 39.0 mm.

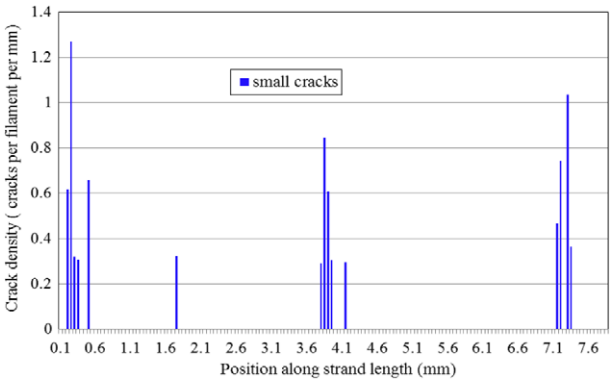

Figure 20. Distribution of the crack density along the strand length of the OST-1 (IT) strand after applied periodic peak bending strain with cylinder C.

sample after cyclic testing [14]. The conductor is cabled from the same strand as discussed above and indicated as OST-1. One specimen with a length of 190 mm is taken from the section subjected to large electromagnetic load in the high magnetic field region and the other section with a length of 250 mm is cut from the lowest magnetic field, near the upper terminations. The sample taken from the high magnetic field region is subjected to electromagnetic load cycling and showed a considerable degradation of the current sharing temperature. Both samples were measured with the Twente AC-dipole magnetization measurement setup [10]. The AC loss measurements were carried out at liquid helium temperature (4.2 K, atmospheric pressure bath) and with a perpendicular applied sinusoidal magnetic field having a bipolar amplitude B_a of 1 T (no offset) and with frequency ranging from 1 to 30 mHz.

The results of the experimental AC loss comparison between the highly degraded conductor sample and the section taken from the low-field zone is presented in figure 18. It shows that there is no noticeable difference in hysteresis loss, but as expected only in the coupling loss. The maximum uncertainty in the determination of the hysteresis loss at the intersection with zero frequency for this first limited set of CICC data is relatively high and amounts to ±4%. The coupling loss in the section of the full-size ITER TF sample subjected to the high-field load cycling was reduced by 36% compared to that of the low-field sample. This difference is mainly attributed to an increase of the interstrand resistance due to the strand disengagement during cyclic loading [14–16, 27].

The amount of filament cracks observed in the TARSIS samples tested up to a peak bending force of 10 kN m^{-1} is analyzed in collaboration with the ASC group at the Florida State University. For ITER Nb_3Sn internal-tin samples tested in TARSIS and afterwards analyzed on filament crack distribution, it appeared that no cracks were observed when loaded up to 6 kN m^{-1}, which corresponds to a peak bending strain of about 1% [28]. Cracks were only found in samples loaded up to 10 kN m^{-1} (peak bending strain of about 1.5%). It should be noted that the peak bending strain is defined as the maximum strain at the outer region of the filamentary zone and most filaments in the wire cross-section are subjected to much lower strain.

In addition to the bending of the AC loss samples with cylinders A and B, we performed a bending test on the OST-1 wire with a cylinder having a diameter of 39.0 mm. This resulted in a hysteresis loss reduction of 5% (see figure 19) and a crack pattern as shown in figure 20.

Based on the revealed correlation between the growth of microscopic filament cracks and decrease in hysteresis loss as observed in the OST-1 strand, we can say that if cracks are present in the degraded full-size CICC sample, the peak crack concentration is at least less than 1 cracks/mm/filament. This corresponds to an average crack density for the OST-1 wire of 0.05 cracks/mm/filament when the whole strand volume is taken into account (see figure 20). It is obvious that not only the average crack density but also the local crack distribution is important for the hysteresis loss reduction. This level of crack density can only be expected in the unlikely case, considering the extreme of the error bar in the hysteresis loss measurement of the full-size CICCs, indicated in figure 18. Most likely the amount of cracks is much less, as the back extrapolations of both AC loss versus frequency curves in figure 18 coincide well at zero frequency. It should be noted that the periodicity in the crack density in our AC loss strand samples is about 5 mm, which is practically in the same range as the expected wavelength in the TFPRO2-OST1 with

ITER Option 1 cable pattern [7, 29]. The strong similarity in the extrapolated values for hysteresis loss of both CICC samples suggests that the large degradation as observed during the cyclic loading test in SULTAN [14] should originate from periodic filament strain variations due to plastic strand deformation and, if present, a restricted amount of filament cracks, instead of a significant amount of distributed filament cracks. The solution against this degradation is obviously to limit the degree of strand deformation connected with bending along a short beam length and interstrand contact stress along point contacts due to electromagnetic and thermo-mechanical loading to the utmost minimum [7, 29].

A better quantitative assessment of the number of cracks in CICCs can be attained by improving the accuracy of the AC loss measurement on the full-size CICC and also by extending the strand characterization.

7. Conclusions

We found a clear correlation between microscopic filament fracture, coupling and hysteresis AC losses in the investigated Nb_3Sn strands.

For typical ITER type internal-tin strands, (except the RRP OST-Dipole strand), the reduction in hysteresis loss is about 30% for an average crack density of 1 crack/filament/mm. It seems that cracks reduce the effective filament diameter for hysteresis loss due to breaking of the superconducting loops that were established by the bridging among filaments. Other strand types, where bridging does not occur (PIT or RRP type of strand), do not show a clear decrease in hysteresis loss.

In the tested ITER type bronze strand, we observed longitudinal cracks in the filaments that not only reduce the real filament dimensions but also the effective filament diameter. The density and size of the longitudinal cracks increases with applied bending strain.

The coupling loss also decreases with the growth of filament cracks, depending on the strand processing method.

An example is given for use of AC loss measurement as a method to evaluate the number of cracks in an ITER TF type Nb_3Sn CICC. The hysteresis loss of a cycled and degraded section of a CICC sample from the high magnetic field zone is compared to that of a section from the low-field zone, indicating that the amount of cracks is constrained but the method is limited by the accuracy of the hysteresis loss determination. The maximum error bar in the AC loss measurement allows at utmost an average crack density of 0.05 cracks/filament/mm and a peak crack density of 1 cracks/filament/mm, but it seems reasonable to expect a smaller amount in reality.

References

[1] Ekin J W 1981 *Superconducting Materials Science—Metallurgy, Fabrication and Applications* (New York: Plenum)
[2] Mitchell N 2003 *Fusion Eng. Des.* **66–68** 971–93
[3] Ekin J W 1984 *Adv. Cryogenic Eng.* **30** 823–36
[4] Miyoshi Y, van Lanen E P A, Dhallé M and Nijhuis A 2009 *Supercond. Sci. Technol.* **22** 085009
[5] Jewell M C, Lee P J and Larbalestier D C 2003 *Supercond. Sci. Technol.* **16** 1005–11
[6] Nijhuis A, Ilyin Y, Wessel W A J and Abbas W 2006 *Supercond. Sci. Technol.* **19** 1136–45
[7] Nijhuis A and Ilyin Y 2006 *Supercond. Sci. Technol.* **19** 945–62
[8] Nijhuis A *et al* 2005 *Supercond. Sci. Technol.* **18** S273–83
[9] de Reuver J L 1985 AC losses in current-carrying superconductors *PhD Thesis* University of Twente
[10] Verweij A P 1995 Electrodynamics of superconducting cables in accelerator magnets *PhD Thesis* University of Twente
[11] Campbell A M 1995 *IEEE Trans. Appl. Supercond.* **5** 682–7
[12] Ries G 1977 *IEEE Trans. Magn.* **13** 524–6
[13] Goldfarb R B and Itoh K 1994 *J. Appl. Phys.* **75** 2215–118
[14] Bruzzone P *et al* 2008 *IEEE Tran. Appl. Supercond.* **18** 1088–91
[15] Nijhuis A, Ilyin Y, Abbas W, ten Kate H H J, Ricci M V and della Corte A 2005 *IEEE Trans. Appl. Supercond.* **15** 1633–6
[16] Nijhuis A, Ilyin Y, Abbas W, ten Haken B and ten Kate H H J 2004 *IEEE Trans. Appl. Supercond.* **14** 1489–94
[17] Nijhuis A, Miyoshi Y, Jewell M C, Abbas W and Wessel W A J 2009 *IEEE Tran. Appl. Supercond.* **19** 2628–32
[18] Mitchell N 2003 *Cryogenics* **43** 255–70
[19] Mitchell N 2007 *Supercond. Sci. Technol.* **20** 25–34
[20] Miyoshi Y, van Lanen E P A, Dhallé M and Nijhuis A 2010 *IEEE Trans. Appl. Supercond.* **20** 1404–7
[21] Ghosh A K, Robins K E and Sampson W B 1985 *IEEE Trans. Magn.* **21** 328–31
[22] Goldfarb R B and Ekin J W 1986 *Cryogenics* **26** 478–81
[23] Ghosh A K *et al* 2005 *IEEE Trans. Appl. Supercond.* **15** 3494–7
[24] Bordini B *et al* 2011 *IEEE Trans. Appl. Supercond.* **21** 3373–6
[25] Lee P J, Sheth M, Tarantini C, Sanabria C, Novelli C, Escobedo D, Starch B and Larbalestier D 2011 ITER TF strand characterization at FSU *3rd ITER Conductor Reconsilliation Workshop (Aix, France, June 2011)*
[26] Wilson M N *et al* 1970 *J. Phys. D: Appl. Phys.* **3** 1517–85
[27] van Lanen E P A, Feng L, Pompe van Meerdervoort R P, Wessel W A J and Nijhuis A 2010 *IEEE Trans. Appl. Supercond.* **20** 474–7
[28] Sanabria C *et al* 2011 Metallographic examination of filament fracture in ITER Nb_3Sn TF strands after transverse and axial loading tests *CEC-ICMC (Spokane, WA, June 2011)*
[29] Nijhuis A, van Lanen E P A and Rolando G 2012 *Supercond. Sci. Technol.* **25** 015007